Article

Simulation of Fluid Flow and Inclusion Removal in Five-Flow T-Type Tundishes with Porous Baffle Walls

Shuo Zhao [1,*], Shibin Zhu [1], Yangyang Ge [1], Jianfeng Wang [1], Dong Xu [1], Zushu Li [2] and Chao Chen [3]

[1] Technology Innovation Center for High Quality Cold Heading Steel of Hebei Province,
    Department of Materials Science and Engineering, Hebei University of Engineering, Handan 056000, China
[2] Warwick Manufacturing Group, The University of Warwick, Coventry CV4 7AL, UK
[3] Department of Metallurgy, Taiyuan University of Technology, Taiyuan 030024, China
[*] Correspondence: zhaos418@hebeu.edu.cn

Abstract: To solve the instability of liquid steel in the continuous casting process and the inconsistent flaw detection of heavy rail steel, steel flow control was studied numerically in a tundish with a porous baffle wall by using the fluid dynamics software Fluent. The opening plan of the baffle wall was improved through orthogonal optimization of the design of the holes in the porous baffle wall. The test condition was set to a left inclination angle of $\alpha_1 = 22°$, a right inclination angle of $\alpha_2 = 48°$, an upward elevation angle of $\beta = 30°$, and an aperture of $d = 70$ mm. The simulation results of the optimization scheme showed that the uniformity of the flow and temperature fields had been significantly improved, and the flow in each strand became consistent. The maximum temperature difference was 21 K in the tundish, and the maximum temperature difference of three outlets was only 1.7 K. Dead zone volume was reduced by 10.0% compared to the original tundish, and plug flow volume was increased by 14.2%. Comparing the removal efficiency of Al_2O_3 inclusions of different size, the results showed that the removal efficiency of 10 μm and 30 μm smaller inclusions was above 87%. The removal rate of ≥ 50 μm larger inclusions also remained about 95%.

Keywords: five-strand tundish; numerical simulation; flow control; fluent

1. Introduction

In the continuous casting process, the tundish not only plays a role in storage, the buffering and diverting of molten steel, and continuous casting, but also plays an important role by preventing slag from entering the mold, homogenizing temperature and steel composition, and improving the removal rate of non-metallic inclusions in steel [1–4]. With improvements in CFD (computational fluid dynamics) software and the enhancement of computing capacity, numerical simulation occupies an increasingly important position in continuous casting [5,6] and provides a lot of convenience for related fields, which has thus led to it being favored by many scholars. Chen et al. reported on the mathematical modeling of different tracers in a casting tundish [7–10]. Holzinger showed flow interaction in a casting tundish due to bubble curtain operation [11], and Cwudzinski introduced the physical and mathematical modeling of the behavior of bubble plumes in a one-strand tundish [12]. In order to improve the quality of molten steel, Chang et al. pointed out that the modeling of inclusion removal using micro-bubble swarms in a full-scale tundish is very useful [13]. In recent years, with the rapid development of high-speed rail, the quality requirements of railway tracks are constantly expanding. As the main material of high-speed rail, heavy rail steel needs to have high strength, toughness, and wear resistance. In order to improve the purity and comprehensive performance of heavy rail steel, it is increasingly important to study the casting tundish in order to improve the castability of molten steel and slab quality [14,15]. However, research on the flow field optimization of T-type tundishes for application in the casting of heavy rail steel is relatively rare. In order

to solve the practical problems of a heavy rail steel plant, it is particularly urgent that a suitable tundish structure is designed.

By establishing a three-dimensional mathematical model of flow and heat transfer in tundishes, the structural optimization of a five-flow T-type continuous casting tundish was studied in this paper. The flow field and temperature field were solved using ANSYS Fluent 17.0 (ANSYS Inc., Canonsburg, PA, USA), and the results were analyzed by ANSYS CFD-POST (ANSYS Inc., Canonsburg, PA, USA) and Tecplot software (Tecplot Inc., Bellevue, WA, USA). Due to the existing problems in the original structure of the tundish, a porous retaining wall was added on the turbulence controller to improve the structure of the tundish. The influence of the combination of "turbulence controller + retaining wall" on fluid flow in the tundish was studied, and orthogonal design was used to optimize the structure of the porous retaining wall. The flow field, temperature field, and level of inclusion removal in the improved tundish were analyzed to obtain the optimal parameters.

2. Basic Theory and Method

2.1. Fundamental Assumption

The flow of molten steel in tundishes is a very complex turbulent flow that is accompanied by complex physical and chemical reactions, and the movement of inclusions is subject to random turbulent fluctuations. Some necessary assumptions are made for the flow, heat transfer, and inclusion of molten steel [16–18]:

(1)　Liquid steel is an incompressible viscous fluid. The flow of molten steel is that of a high-Reynolds number steady-state turbulent flow. Assuming that the liquid surface is a free-slip surface, the effects of liquid surface fluctuation and surface covering agent on flow are ignored.

(2)　Heat transfer is a three-dimensional steady-state process. The effect of temperature change on the relevant physical parameters of molten steel is ignored.

(3)　The inclusions are assumed to be spherical, and the particle diameters are set as 10 μm, 30 μm, 50 μm, 70 μm, and 90 μm. Without considering collision polymerization and wall adsorption, it is considered that inclusions are absorbed by the slag layer when they reach the liquid steel surface.

2.2. Control Equation

The relevant equations are provided below.

Continuity equation:

$$\frac{\partial(\rho u_i)}{\partial x_i} \tag{1}$$

Momentum equation:

$$\frac{\partial(\rho \mu_i \mu_j)}{\partial x_j} = -\frac{\partial P}{\partial x_j} + \frac{\partial}{\partial x_j}\left(\mu_{eff}\frac{\partial \mu_i}{\partial x_j}\right) + \frac{\partial}{\partial x_i}\left(\mu_{eff}\frac{\partial \mu_i}{\partial x_i}\right) + \rho g_i \tag{2}$$

Energy equation:

$$\rho C_p\left(u\frac{\partial T}{\partial x} + v\frac{\partial T}{\partial y} + w\frac{\partial T}{\partial z}\right) = \frac{\partial}{\partial x}\left(k_{eff}\frac{\partial T}{\partial x}\right) + \frac{\partial}{\partial y}\left(k_{eff}\frac{\partial T}{\partial y}\right) + \frac{\partial}{\partial z}\left(k_{eff}\frac{\partial T}{\partial z}\right) \tag{3}$$

Turbulent kinetic energy equation:

$$\frac{\partial(\rho u_i k)}{\partial x_i} = \frac{\partial}{\partial x_i}\left[\left(u_{eff} + \frac{u_t}{\sigma_k}\right)\frac{\partial k}{\partial x_i}\right] + G - \rho\varepsilon \tag{4}$$

Turbulent kinetic energy dissipation rate equation:

$$\frac{\partial(\rho u_i \varepsilon)}{\partial x_i} = \frac{\partial}{\partial x_i}\left[\left(u_{eff} + \frac{u_t}{\sigma_\varepsilon}\right)\frac{\partial \varepsilon}{\partial x_i}\right] + \frac{c_1\varepsilon G - c_2\rho\varepsilon^2}{k} \tag{5}$$

$$G = u_t \frac{\partial u_j}{\partial x_i} \left(\frac{\partial u_i}{\partial x_j} + \frac{\partial u_j}{\partial x_i} \right) \tag{6}$$

$$u_{eff} = \mu + u_t = \mu + c_u \rho \frac{k^2}{\varepsilon} \tag{7}$$

Tracer transport equation:

$$\rho \frac{\partial c}{\partial t} + \rho u_i \frac{\partial c}{\partial x_i} = \frac{\partial}{\partial x_i} \left(\rho D_{eff} \frac{\partial c}{\partial x_i} \right) \tag{8}$$

$$D_{eff} = D_0 + \frac{u_{eff}}{\rho Sc_t} \tag{9}$$

In the above expressions, u_i, u_j is the direction represented by the tensor m·s^{-1}; P represents fluid density, kg·(m^3)$^{-1}$; T is fluid temperature, K; C_P is effective heat capacity, J·(kg·K)$^{-1}$; k_{eff} is the effective heat transfer coefficient, W·(m·K)$^{-1}$; μ is the fluid viscosity coefficient, kg·(m·s)$^{-1}$; μ_t is an additional viscosity coefficient of fluid, kg·(m·s)$^{-1}$; k is turbulent kinetic energy, m^2·(s^2)$^{-1}$; ε is turbulent kinetic energy dissipation rate, m^2·(s^3)$^{-1}$; D_{eff} is the effective diffusion coefficient, kg·(m·s)$^{-1}$; c is tracer concentration, kg·(m^3)$^{-1}$; Sc_t is the Schmidt number of the tracer; and D_0 is the tracer diffusion coefficient, m^2·s^{-1}. Where C_1, C_2, C_u, σ_k, σ_ε is a constant, the values recommended by Launder and Spalding are used [19,20]:

$$c_1 = 1.43; \ c_2 = 1.92; \ c_u = 0.09; \ \sigma_k = 1.00; \ \sigma_\varepsilon = 1.30$$

2.3. Inclusion Motion Equation

The trajectory of inclusions in the tundish satisfies the Euler–Lagrange particle tracking model. In general, after the convergence and stability of the steady flow field calculation, the corresponding model of inclusions is calculated by Fluent, and the influence of drag and buoyancy on inclusions should be considered. The equations are as follows:

$$\frac{d\bar{u}_p}{d_t} = F_D \left(u_i - u_p \right) + \frac{(\rho_p - \rho)}{\rho_p} g_i \tag{10}$$

$$F_D = \frac{18\mu_0 C_D R_e}{24\rho_p D_p{}^2} \tag{11}$$

In the formula, u_p represents inclusion particle velocity per hour, m·s^{-1}; ρ_p represents inclusion density, kg·(m^3)$^{-1}$; F_D denotes drag, N; and C_D is the drag coefficient.

3. Grid and Boundary Conditions

3.1. Model Grid

The research object is a five-strand T-shaped continuous casting tundish. Since the structure of the tundish is symmetrical, half of the tundish is taken for calculation when obtaining the results. The three-dimensional model of the tundish is shown in Figure 1, and the three outlets are marked as 1#, 2#, and 3#.

The basic simulation parameters stem from the specified data provided by the production site and are listed in Table 1.

The mesh of the model was obtained through ANSYS Meshing, and the mesh is unstructured with a tetrahedral and hexahedral combination. In order to improve the accuracy of simulation calculation, grid refinement and encryption were carried out at positions with a large gradient of turbulence intensity parameters, such as inlets, outlets, and relevant flow control positions, and boundary layer grid division was carried out on the relevant wall boundary to meet the requirements of calculation accuracy and wall

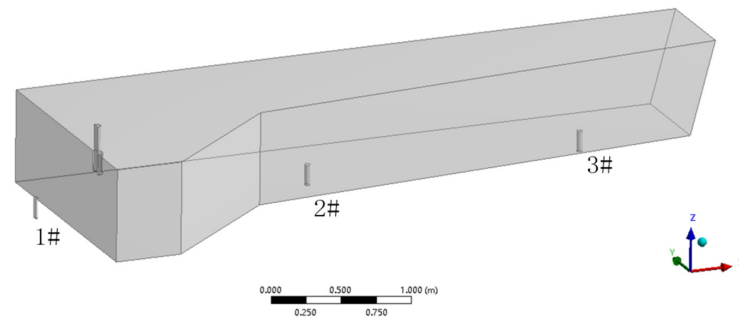function. Finally, the number of grids was about 250,000. The model grids are shown in Figures 2 and 3.

Figure 1. 3D model of the tundish.

Table 1. Basic parameters.

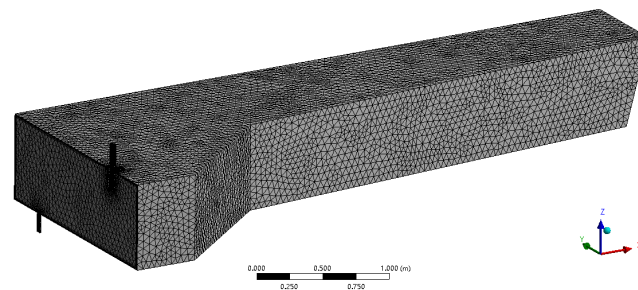| Parameters	Values	Parameters	Values
Inlet diameter, mm	65	Speed, m·min^{-1}	0.5
Outlet diameter, mm	40	Steel density, kg·(m^3)$^{-1}$	7100
Strand spacing, mm	2096	Steel viscosity, Pa·s	0.0062
Immersion depth, mm	150	Thermal conductivity, W·(m·K)$^{-1}$	740
Liquid level, mm	680	Specific heat capacity, J·(kg·K)$^{-1}$	41
Slab size, mm	380 × 280	Inclusion density, kg·(m^3)$^{-1}$	5000

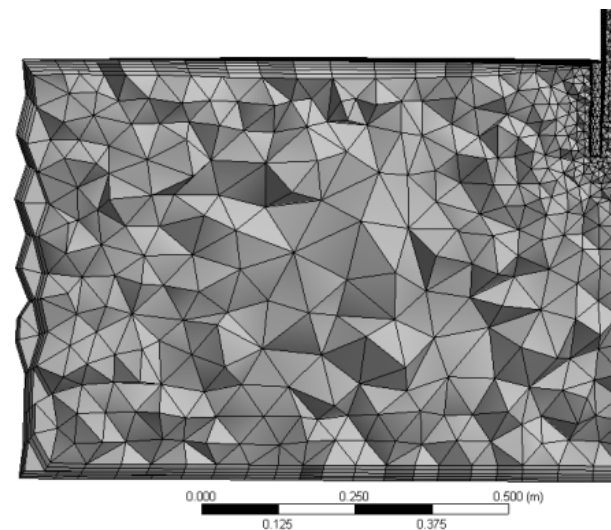**Figure 2.** Model mesh.

Figure 3. Inlet cross section grid.

3.2. Boundary Condition

(1)　Inlet boundary condition:

The velocity inlet is selected as the boundary condition of the model's inlet. The velocity direction is perpendicular to the long nozzle plane and evenly distributed across the whole nozzle plane.

(2)　Outlet boundary condition:

The boundary condition of the outlet is set as a free flow boundary to ensure the full flow of molten steel in the tundish.

(3)　Wall boundary condition:

The upper surface of the molten steel is set as a free-slip wall that ignores the influence of liquid level fluctuation and covering agent, and the variable gradient in the vertical direction is zero. The rest walls are set as non-slip walls, and the heat transfer conditions of each wall are set.

(4)　Symmetric boundary:

The model's symmetric surface is defined as the symmetric boundary, and the velocity and normal gradient of other variables on this surface are zero.

4. Numerical Simulation of Adding a Porous Baffle Wall

4.1. Structural Design

Porous baffle walls are a device with a significant flow control effect, which can improve the flow field of multi-flow tundish, maintain uniform steel composition and temperature, and promote inclusion removal. Previous studies [21–23] have shown that the structural design of porous baffle walls mainly focuses on factors such as shape, hole number, aperture, relative position, and the inclination angle of holes. Therefore, the influence of four factors on the flow control effect of porous baffle walls are focused upon in this experiment, namely aperture d, horizontal angle α_1, horizontal angle α_2, and elevation angle β. Next, combined with the actual parameters, the baffle wall structure was designed.

(1)　Shape:

The distance between the U-shaped baffle wall and the outlet center line was 300 mm, as shown in Figure 4.
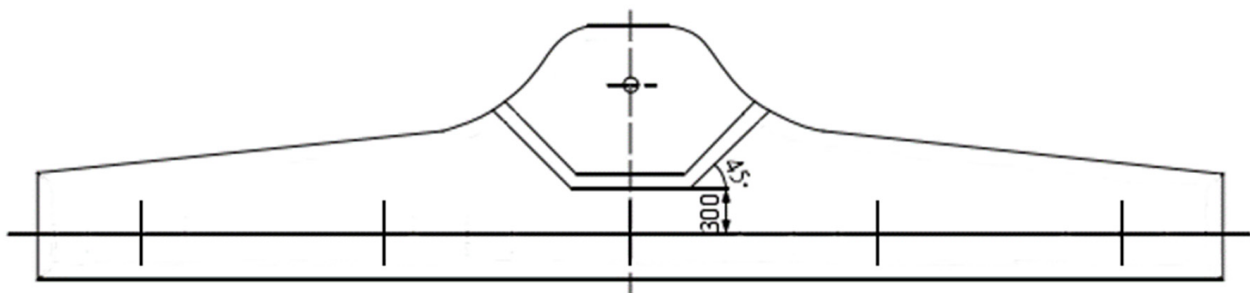

Figure 4. Schematic diagram of the shape of the porous baffle wall.

(2)　Hole number:

According to the literature [21,24,25], for multi-flow tundishes, the number of holes on one side of the baffle wall is generally three or four.

(3)　Hole position:

In order to ensure the stability of the retaining wall [24,25], flow control, and liquid level, the hole positions of the porous baffle wall were carefully designed, and the schematic diagram is shown in Figure 5. The positions were as follows: l_1 = 300 mm, l_2 = 350 mm, l_3 = 250 mm, and l_4 = 200 mm. Among these positions, l_3 is determined by l_2.
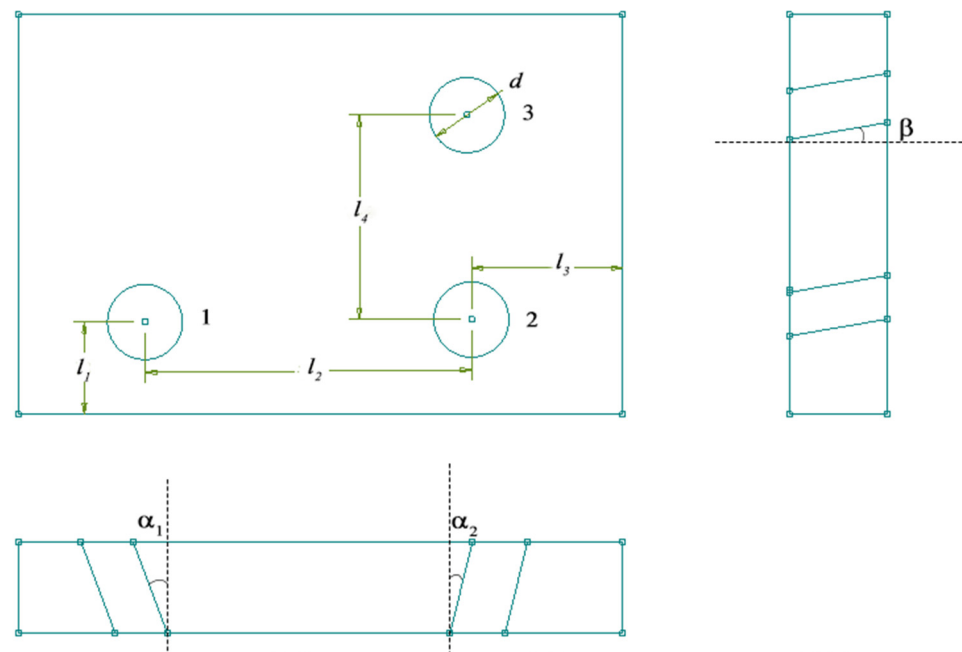
Figure 5. Schematic diagram of openings in the porous baffle wall.

(4)   Hole diameter:

According to the relevant literature [24,26], the recommended diameter of baffle wall holes (d) is 70–100 mm.

(5)   Hole inclination angle:

A three-dimensional model of the porous tundish baffle wall is shown in Figure 6. The sizes of the three diversion holes are consistent. According to the flow characteristics of molten steel and the temperature field distribution, the left horizontal inclination α_1 of the first hole is in the range of 20–50°, the right horizontal inclination α_2 of the second and third holes is in the range of 40–55°, and the elevation angle β of the three holes is in the range of 20–35°.
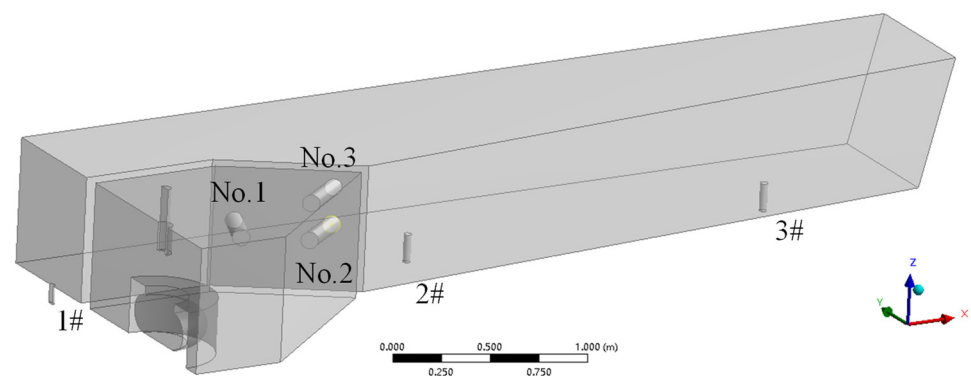
Figure 6. Model of the tundish with a porous baffle wall.

4.2. Orthogonality Design Plan

In this study, orthogonal analysis was used to explore the effects of different factors and levels on the flow field and temperature field of the tundish. There were four factors affecting the flow control effect of baffle walls in the scheme and four different levels were taken for each factor, thus forming a 4 × 4 orthonormal table, as shown in Table 2.

Table 2. Orthogonal design for diversion holes.

No.	Left Angle α_1/°	Right Angle α_2/°	Vertical Angle β/°	Hole Size d/mm
1	22	40	20	70
2	30	44	25	70
3	38	48	30	70
4	46	52	35	70
5	46	48	25	80
6	38	44	20	80
7	30	40	35	80
8	22	52	30	80
9	22	48	35	90
10	30	52	20	90
11	38	40	25	90
12	46	44	30	90
13	46	40	30	100
14	38	52	35	100
15	30	48	20	100
16	22	44	25	100
17	30	44	35	100
18	30	52	30	100
19	46	52	25	100
20	46	52	20	100

4.3. Orthogonal Analysis Results

Numerical simulation of the 20 schemes listed in Table 2 was performed, and the best baffle wall opening scheme was determined by orthogonal analysis. In evaluating the flow control effect of the porous baffle wall, it was necessary to select representative indexes for orthogonal analysis. In this study, the average residence time, the starting response time, the overall average residence time, and the consistency with which each outlet in the tundish could be cast were used as the orthogonal analysis indexes. The consistency with which each outlet could be cast was measured by the comprehensive standard deviation of average residence time (S). With the variances in the average residence time of the 1#, 2#, and 3# flows denoted by S_1, S_2, and S_3, then

$$S = \sqrt{\frac{S_1 + S_2 + S_3}{3}} \qquad (12)$$

The simulation results for the orthogonal scheme were counted according to the above indexes, as shown in Table 3. Among them, t_1, t_2, and t_3 are the average residence time of outlet 1#, 2#, and 3#, respectively. t_{avg} is the total average residence time. t_{min} is the starting response time. S is the combined standard deviation of the average residence time of each flow.

Table 3. Simulation results of the orthogonal scheme of the porous baffle wall.

No.	t_1/s	t_2/s	t_3/s	t_{avg}/s	t_{min}/s	S
1	1576	1569	1775	1644	64	95.6
2	1535	1541	1841	1646	57	138.2
3	1541	1627	1765	1644	62	92.3
4	1496	1677	1762	1645	59	110.9
5	1464	1662	1751	1646	56	120.0
6	1448	1624	1869	1647	61	172.6
7	1499	1618	1814	1644	59	129.9
8	1541	1641	1753	1645	63	86.6
9	1561	1581	1771	1644	68	89.6
10	1562	1665	1662	1648	71	52.6

Table 3. *Cont.*

No.	t_1/s	t_2/s	t_3/s	t_{avg}/s	t_{min}/s	S
11	1494	1576	1896	1646	65	178.5
12	1534	1612	1790	1645	67	107.2
13	1470	1612	1856	1646	65	159.4
14	1430	1623	1884	1646	57	186.0
15	1603	1608	1831	1646	65	137.8
16	1539	1521	1874	1645	55	176.5
17	1509	1655	1765	1643	67	104.9
18	1480	1614	1844	1646	53	150.3
19	1495	1795	1662	1647	48	135.1
20	1458	1822	1662	1647	47	149.0

In order to determine the best opening scheme for the designed porous baffle wall, the orthogonal analysis results showed that:

(1) The left inclination angle α_1 of the first hole has a significant effect on the comprehensive standard deviation of start response time and average residence time. The left angle α_1 controls the flow of molten steel near outlets 1# and 2#. Because the first hole is located between outlets 1# and 2#, the molten steel from the diversion hole flows directly from the molten steel surface to these two outlets. Therefore, when the left angle α_1 becomes large, the first hole is closer to outlet 1# outlet, and shortening the distance between them will shorten the starting response time of the molten steel at the corresponding outlet. At the same time, the increase in the left angle α_1 will incline the flow direction of molten steel more toward outlet 1# and increase the standard deviation of the average residence time of the three outlets, which is not conducive to the flow consistency of molten steel.

(2) The right angle α_2 of the second and third holes mainly regulates the flow in the relevant area of distal outlet 3#. In order to ensure that the molten steel can also maintain flow consistent with outlets 1# and 2# at the farthest end, it is necessary to guide the molten steel in the injection area to the distal end of the tundish with the right angle α_2. With increases in the right angle α_2, the standard deviation of average residence time decreases gradually and the consistency of each flow is greatly improved. However, when α_2 is too large, it will also cause excessive flow to the distal end of molten steel and make the flow of outlets 1# and 2# become worse; therefore, it is important that the right angle α_2 has the appropriate value.

(3) With increases in aperture d, the flow control effect of the diversion hole will be weakened, which is not conducive to improving the flow consistency of molten steel. When aperture is at the minimum level, the comprehensive standard deviation of average residence time is small and flow consistency is good.

(4) Increases in elevation angle β will prolong the flow path and residence time of molten steel, but the effect is not obvious. By analyzing the average residence time of each outlet, it can be clearly seen that the average residence time of outlet 3# is no longer greater than the theoretical residence time, and the average residence time of outlets 1# and 2# is significantly increased, which is the interaction between the elevation angle β and the horizontal inclination angles α_1 and α_2.

Under the action of multiple factors and levels, average residence time and the comprehensive standard deviation of each flow change greatly, while the fluctuation in total average residence time and start response time is small. When the optimal level of each factor was considered, the consistency of each outlet was taken as the main reference, and a baffle wall hole with a left inclination angle $\alpha_1 = 22°$, right inclination angle $\alpha_2 = 48°$, upper elevation angle $\beta = 30°$, and aperture $d = 70$ mm was adopted.

4.4. Flow Field of the Tundish

Numerical simulation of the tundish with a porous baffle wall was carried out according to the best opening scheme, and the flow field simulation results are shown in Figure 7.
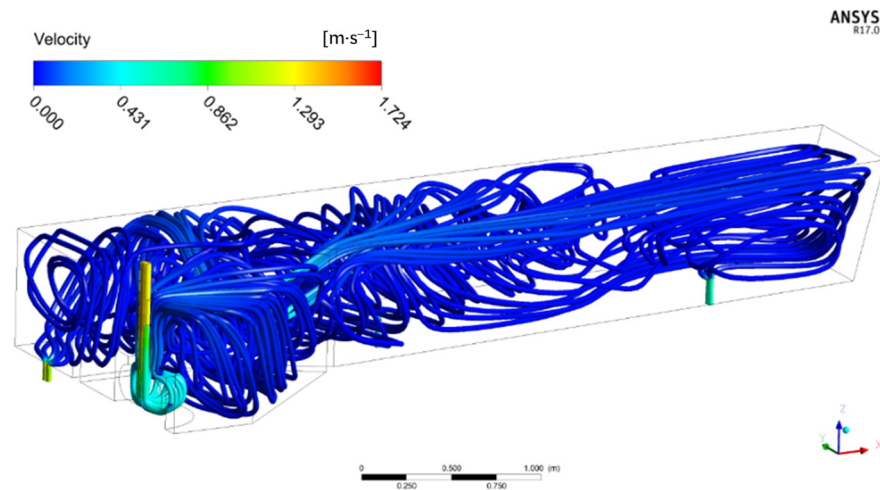

Figure 7. Streamline diagram of the tundish.

The diversion hole in the baffle wall has the function of distributing and guiding the molten steel in the injection area. The molten steel flows to each outlet of the tundish under the action of the diversion hole, and there are no cases where the molten steel is too biased towards a certain outlet. Compared to the single turbulence controller, the liquid velocity distribution of the molten steel surface in the injection area is more uniform with a baffle wall, and the maximum velocity of the liquid surface is smaller with less fluctuation. In the injection area, the velocity of the molten steel near the second and third holes is slightly higher due to molten steel being aggregated by the holes (maximum velocity is 0.12 m·s^{-1}). The velocity distribution at the far end of the molten steel surface is obviously better, and the molten steel through the second and third diversion holes extends to the far end at a great speed, which thus optimizes the far end speed too slowly (an important factor when seeking to improve the consistency of each flow). The diversion hole makes the molten steel flow more uniform and greatly reduces the generation of vortex flow. The molten steel can thus fully flow in all regions of the tundish, which is also of great significance in terms of inclusion removal.

4.5. Residence Time Distribution Curve of the Tundish

Numerical simulation of the residence time distribution (RTD) curve for the tundish with a porous baffle wall demonstrates that the porous baffle wall significantly improved the consistency of each flow. The calculated results are shown in Figures 8–10. (plan A: no flow control device; plan B: round turbulence inhibitor; plan C: round turbulence inhibitor + dam and weir; plan D: round turbulence inhibitor + porous baffle wall.)

Through analysis of the RTD curve, it can be seen that the flow of the distal three-strand outlet has been greatly improved, and there was no indication that the average residence time of the distal outlet was greater than the theoretical residence time. The residence time of molten steel in outlets 1# and 2# was also improved by 67.7% and 30.3%, respectively. For outlet 1#, it was closest to the injection area before optimization, and the molten steel flowed directly to outlet 1# after being injected from the long shroud. This resulted in a short average residence time for molten steel in outlet 1#, which is not conducive to improving inclusion removal and flow consistency. The molten steel in the injection area was redistributed after the porous baffle wall was installed, which greatly extended the average residence time of the molten steel in outlet 1# and prevented short-circuit flow. Through the flow line of residence time, it can be seen that there was no obvious lag zone for flow in the whole tundish, and the flow lag problem in the corner area was also improved.

In terms of the volume fraction of each zone, the residence time of molten steel at outlets 1# and 2# increased due to the porous baffle wall, and the starting response time of molten steel was also prolonged, which effectively prevented the occurrence of short-circuit flow. Therefore, the volume of the plug flow zone was significantly increased. As the distal flow was more sufficient, dead zone volume decreased by about 10%.
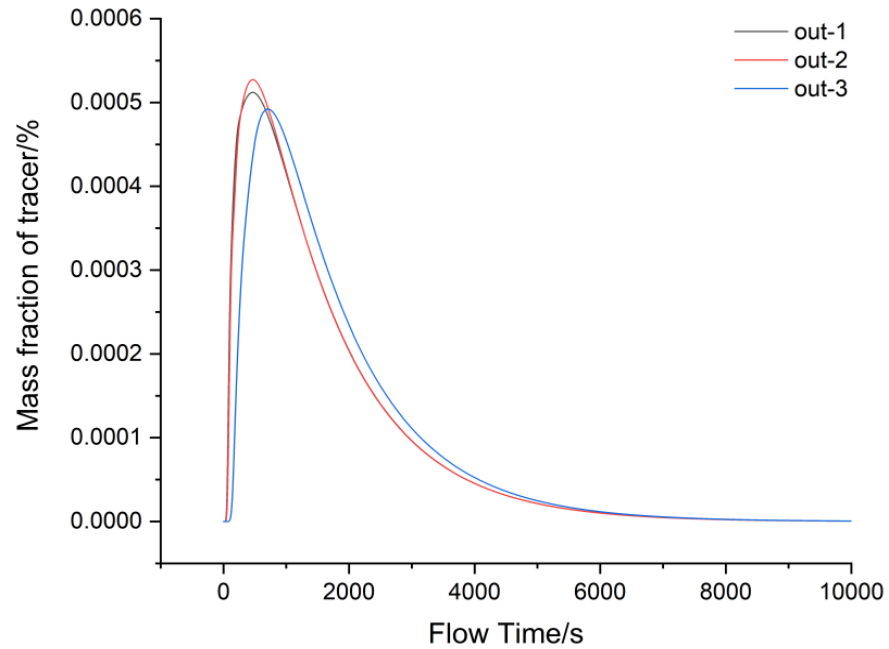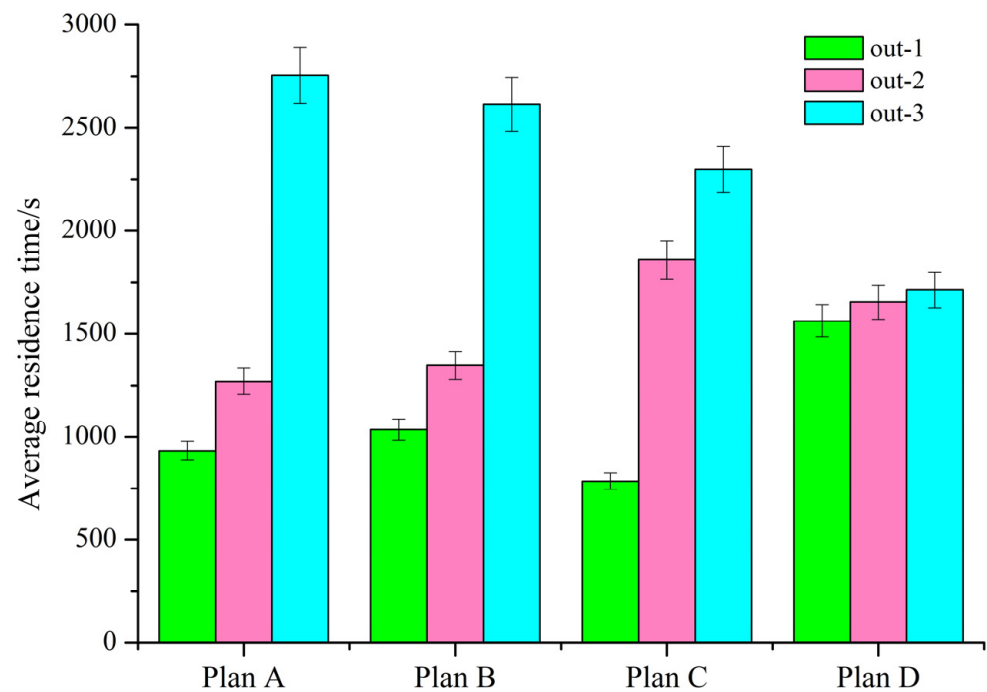

Figure 8. RTD curve of the tundish.

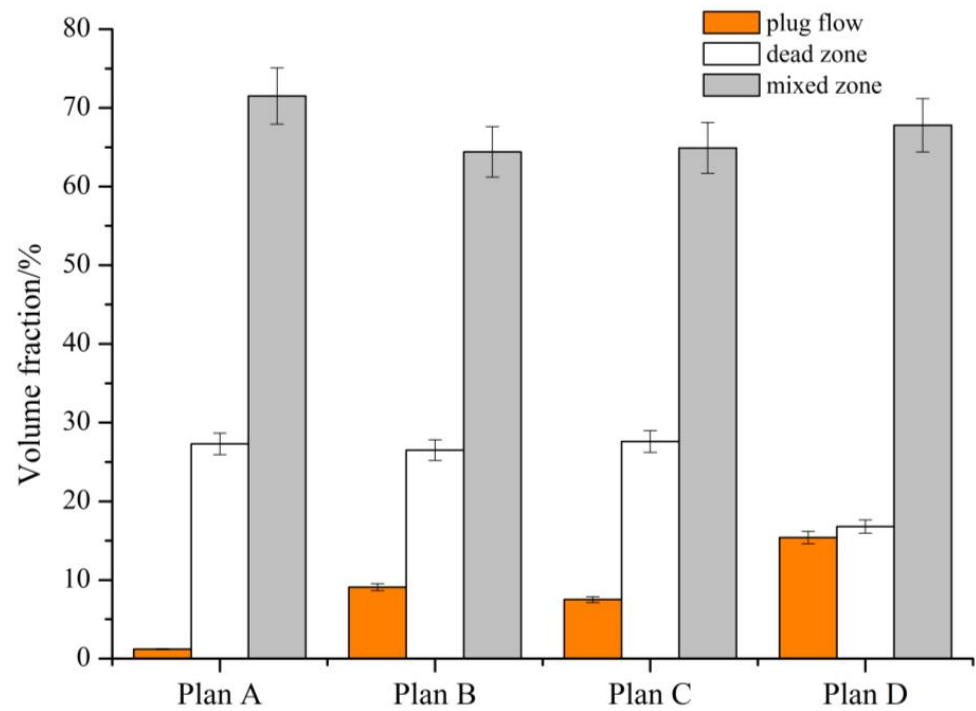**Figure 9.** Average residence time of each outlet.

Figure 10. Volume fraction of each zone.

4.6. Temperature Field of the Tundish

The temperature field of the tundish with a porous baffle wall was numerically simulated, and the corresponding results are shown in Figures 11 and 12. (Plan A: no flow control device; plan B: round turbulence inhibitor; plan C: round turbulence inhibitor + dam and weir; plan D: round turbulence inhibitor + porous baffle wall.)
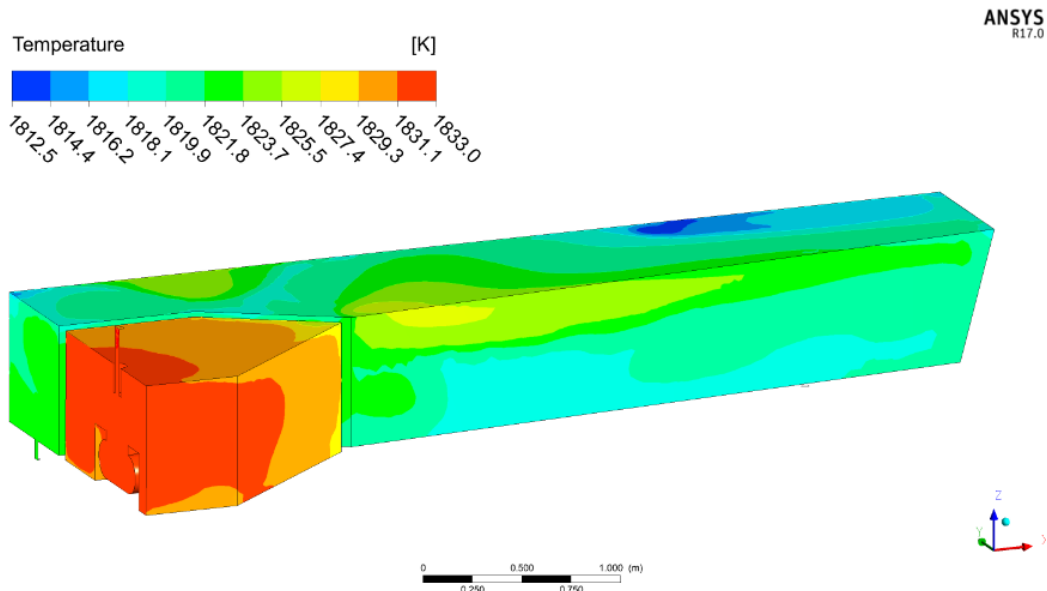

Figure 11. Temperature diagram of the tundish.

The uniformity of the temperature field in the tundish with a porous baffle wall was greatly improved, and the temperature consistency of each outlet was also significantly optimized. The original structure was not able to overcome the low temperature zone in the distal corner. The molten steel flowed slowly near outlet 3#, and the temperature was generally lower than that near outlets 1# and 2#. The temperature in the corner was only

1780 K, the molten steel temperature at outlet 3# was about 1815 K, and the maximum temperature difference between outlet 3# and the other two outlets was more than 10 K. After the porous baffle wall was installed, molten steel flow was comprehensively optimized and molten steel moving at higher speed and of higher temperature also passed the farthest corner region under the influence of the diversion hole. There was no obvious low temperature zone in the tundish and a minimum temperature of around 1812 K was also maintained, which is higher than the temperature before optimization. The temperature of molten steel at the three outlets was 1823.5 K, 1822.5 K, and 1821.8 K. The maximum temperature difference was only 1.7 K, thus the temperature consistency of the three outlets is optimal. The temperature uniformity of molten steel in the tundish is of great significance to composition homogeneity and quality improvement. The overall temperature distribution of the tundish with a porous baffle wall was more reasonable and the temperature fluctuation in the injection area was smaller, which is very beneficial in terms of casting consistency.
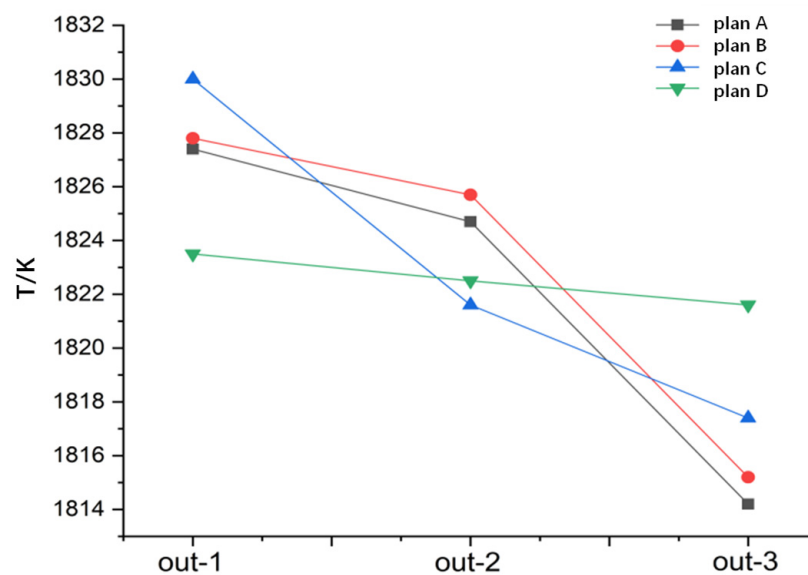

Figure 12. Line diagram of the temperature of each outlet.

4.7. Simulation of Inclusion Removal

After the combined use of a circular turbulence controller and a porous baffle wall, it can be seen that the movement area of inclusions above 50 μm is still concentrated near the injection area (Figure 13). Due to the existence of the baffle wall, it is easier to distinguish the injection area and casting area. Large particles are concentrated and removed in the injection area, and the longest movement time is about 500 s. Small particles (between 10 μm and 30 μm) flow away with molten steel to the distal end under the influence of the diversion hole and movement time is significantly shortened. The longest movement time of 10 μm and 30 μm particles is 1100 s and 780 s, respectively, and the removal rate of small inclusion particles is also higher under this scheme. Although the movement time of small particles is very long before optimization, the removal rate of inclusions is not high. The reason is that the porous baffle wall structure has an obvious improvement effect on the flow field and temperature field, which leads to a fuller flow for molten steel in the tundish. The interaction between different steel flows is enhanced [27], and the removal rate of inclusions of all sizes is improved.
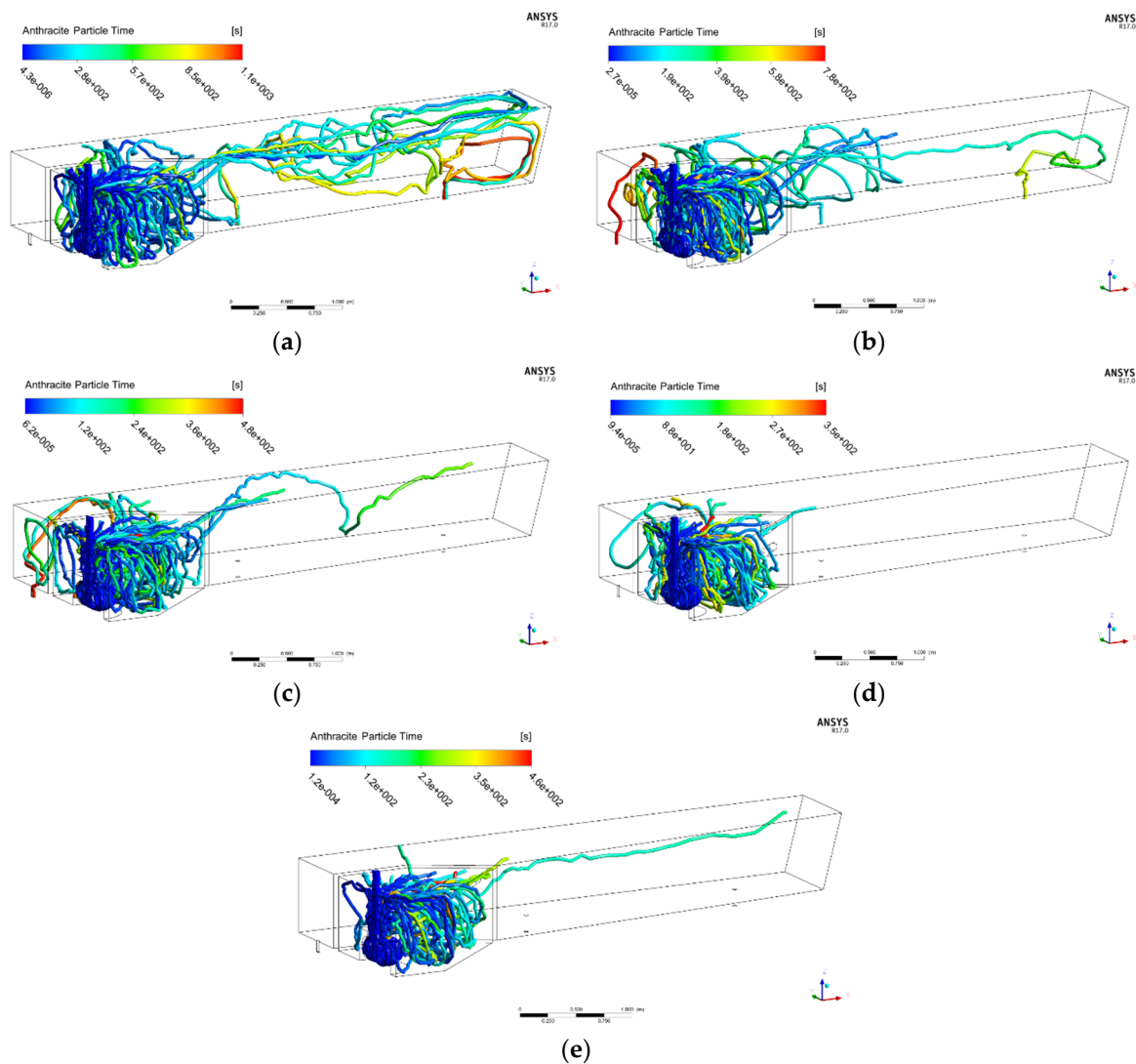
Figure 13. Movement trajectories of five sizes of inclusions. (**a**) 10 μm; (**b**) 30 μm; (**c**) 50 μm; (**d**) 70 μm; (**e**) 90 μm.

5. Conclusions

According to the results from numerical simulation of molten steel in a tundish with a porous baffle wall, the combination of a porous baffle wall and a circular turbulence controller had a better flow control effect for the five-strand T-type tundish. The following conclusions could be drawn:

(1) Compared to before optimization, the uniformity of the temperature field in the tundish was significantly improved by 61.8%, and the flow field of each strand tended to be consistent. The maximum tundish temperature difference was 21 K, and the maximum temperature difference for the three outlets was only 1.7 K. The dead zone volume was 10.0% less than that of the original tundish, and piston zone volume was increased by 14.2%.

(2) The porous baffle wall structure was optimized according to an orthogonal experimental design, and the optimal scheme of baffle wall holes was scientifically analyzed. Finally, the baffle wall opening plan with a left inclination angle of $\alpha_1 = 22°$, right inclination angle of $\alpha_2 = 48°$, upper elevation angle of $\beta = 30°$, and aperture of $d = 70$ mm was selected.

(3) The removal rate of Al_2O_3 inclusions of less than 100 μm in the tundish was calculated. Because there were many problems in terms of the flow of molten steel in the original

tundish, the removal rate of inclusions was not high. The inclusion removal effect of the circular turbulence controller and baffle wall was very obvious. The removal rates of inclusions of all sizes were maintained at more than 80%, and the removal rate of 70 μm and 90 μm inclusions was 98%.

Author Contributions: Conceptualization, S.Z. (Shuo Zhao) and J.W.; methodology, S.Z. (Shuo Zhao); software, Y.G. and S.Z. (Shibin Zhu); formal analysis, Y.G. and S.Z. (Shibin Zhu); investigation, S.Z. (Shuo Zhao); resources, S.Z. (Shuo Zhao); data curation, S.Z. (Shibin Zhu); writing—original draft preparation, S.Z. (Shuo Zhao) and Y.G.; writing—review and editing, S.Z. (Shuo Zhao) and Z.L.; supervision, C.C. and D.X.; project administration, S.Z. (Shuo Zhao); funding acquisition, S.Z. (Shuo Zhao). All authors have read and agreed to the published version of the manuscript.

Conflicts of Interest: The authors declare no conflict of interest.

References

1. Zhao, P.; Zhang, H.; Fang, Q.; Wang, J.H.; Wu, G.L.; Ni, H.W. Numerical study on strand-blocking operation of a six-strand square billet tundish. *J. Iron Steel Res.* **2022**, *34*, 438–450.
2. Neumann, S.; Asad, A.; Schwarze, R. Numerical simulation of an industrial-scale prototypical steel melt tundish considering flow control and cleaning strategies. *Adv. Eng. Mater.* **2020**, *22*, 1900658. [CrossRef]
3. De Sousa, R.J.R.; De Souza, E.E.B.; Marcondes, F.B.; De Castro, J.A. Modeling and computational simulation of fluid flow, heat transfer and inclusions trajectories in a tundish of a steel continuous casting machine. *J. Mater. Res. Technol.* **2019**, *8*, 4209–4220. [CrossRef]
4. Li, E.L.; Feng, K.F.; Guo, H.R.; Sun, J.P.; Zhang, J.Y.; Wang, B. Structure optimization of multi-strand transition piece. *J. Iron Steel Res.* **2022**, *33*, 943–951.
5. Lu, H.B.; Zhong, Y.B.; Ren, Z.M.; Ren, W.L.; Cheng, C.G.; Lei, Z.S. Numerical simulation of EMS position on flow, solidification and inclusion capture in slab continuous casting. *J. Iron Steel Res. Int.* **2022**, *29*, 1807–1822. [CrossRef]
6. Dong, Q.P.; Zhang, J.M.; Yin, Y.B.; Nagaumi, H. Numerical simulation of macrosegregation in billet continuous casting influenced by electromagnetic stirring. *J. Iron Steel Res. Int.* **2022**, *29*, 612–627. [CrossRef]
7. Chen, C.; Jonsson, L.T.I.; Tilliander, A.; Cheng, G.G.; Jönsson, P.G. A mathematical modeling study of tracer mixing in a contin-uous casting tundish. *Metall. Mater. Trans. B* **2015**, *46*, 169–190. [CrossRef]
8. Chen, C.; Jonsson, L.T.I.; Tilliander, A.; Cheng, G.G.; Jönsson, P.G. A mathematical modeling study of the influence of small amounts of KCl solution tracers on mixing in water and residence time distribution of tracers in a continuous flow reactor metallurgical tundish. *Chem. Eng. Sci.* **2015**, *137*, 914–937. [CrossRef]
9. Chen, C.; Ni, P.Y.; Jonsson, L.T.I.; Tilliander, A.; Cheng, G.G.; Jönsson, P.G. A model study of inclusions deposition, macro-scopic transport, and dynamic removal at steel-slag interface for different tundish designs. *Metall. Mater. Trans. B* **2016**, *47*, 1916–1932. [CrossRef]
10. Fan, J.; Li, Y.; Chen, C.; Ouyang, X.; Wang, T.; Lin, W. Effect of uniform and non-uniform increasing casting flow rate on dispersion and outflow percentage of tracers in four strand tundishes under strand blockage conditions. *Metals* **2022**, *12*, 1016. [CrossRef]
11. Holzinger, G.; Thumfart, M. Flow interaction in continuous casting tundish due to bubble curtain operation. *Steel Res. Inter.* **2019**, *90*, 1800642. [CrossRef]
12. Cwudzinski, A. Physical and mathematical modeling of bubbles plume behaviour in one strand tundish. *Metall. Res. Technol.* **2018**, *115*, 2017081. [CrossRef]
13. Chang, S.; Zou, Z.; Li, B. Modeling inclusion removal when using micro-bubble swarm in a full-scale tundish with an impact pad. *Metall. Mater. Trans.* **2022**, *53*, 526–536. [CrossRef]
14. Zhuang, Y.L.; Zhuo, C.; Hao, X.S.; Liu, T.; Sun, Y.H.; Zhang, M. Effect of sulfur content on non-metallic inclusions of heavy rail steel. *Sci. J. Iron Steel Res.* **2022**, *34*, 799–806.
15. Sasai, K. Effect of oxygen and sulfur in molten steel on the agglomeration property of alumina inclusions in molten steel. *ISIJ Inter.* **2018**, *58*, 469. [CrossRef]
16. Li, W.; Jin, Y.; Fang, K.Y. Mathematical model of flow field in tundish with square shape swirl type turbulence inhibitor. *Foundry Technol.* **2018**, *39*, 34–37.
17. Wang, L.T.; Zhang, Q.Y.; Li, Z.B. Study on liquid metal flow and impurity removal inside tundish. *Steelmaking.* **2005**, *21*, 26–29.
18. Liu, G.M.; Bi, X.G.; Jin, Y. Simulation of the inclusion movement in the tundish of slab casting. *Foundry Technol.* **2011**, *5*, 684–687.
19. Launder, B.E.; Spalding, D.B. The numerical computation of turbulent flows. *Comput. Methods Appl. Mech. Eng.* **1974**, *3*, 269–289. [CrossRef]

20. Launder, B.E.; Spalding, D.B. *Mathematical Models of Turbulence*; Academic Press Inc.: London, UK, 1972.
21. Janiszewski, K. Refining of liquid steel in a tundish using the method of filtration during its casting in the CC machine. *Arch. Metall. Mater.* **2013**, *2*, 513–521. [CrossRef]
22. Chang, Z.S. Physical Simulation Study about the Effects of the Double-Baffle with Refractory Fillers on Flow Field in Tundish. Master's Thesis, Wuhan University Science and Technology, Wuhan, China, 2016.
23. Zhong, L.C.; Zhang, L.; Huang, Y.W.; Yang, S.B.; Zhu, Y.X.; Jiang, M.F. Influence of various turbulence inhibitor on fluid flow behavior in tundish. *J. Iron Steel Res.* **2002**, *14*, 6–9.
24. Chen, D.F.; Hu, R.; Wang, Q.X.; Jin, X.; Yan, X.J.; Li, J.Z.; Zhou, K.C. Physical and mathematical study on weir setting in continu-ous casting tundish. *Chin. J. Process Eng.* **2008**, *8*, 49–53.
25. Li, G.Q.; Fu, Y.; Chen, X.H.; Zhang, Z.; Rao, J.P.; Yang, Z.Z. Physical simulation of fluid field and structure optimization in two-strand tundish. *J. Chongqing Univ.* **2015**, *2*, 34–37.
26. Ge, Y.Y. Simulation Research on Flow Field Optimization and Inclusion Removal in Continuous Casting Tundish for Heavy Rail Steel. Master's Thesis, Hebei University of Engineering, Handan, China, 2020.
27. Meijie, Z.; Huazhi, G.; Ao, H.; Hongxi, Z.; Chengji, D. Numerical simulation and industrial practice of inclusion removal from molten steel by gas bottom-blowing in continuous casting tundish. *J. Min. Metall.* **2011**, *2*, 137–147. [CrossRef]